Design, Synthesis, and Characterization of a Novel Blue-Green Long Afterglow $BaYAl_3O_7:Eu^{2+}$, Nd^{3+} Phosphor and Its Anti-Counterfeiting Application

Jiao Wu [1,†], Quanxiao Liu [1,†], Peng Gao [1], Jigang Wang [1,*], Yuansheng Qi [1,*], Zhenjun Li [2,3,*] and Junming Li [4] and Tao Jiang [5]

[1] Beijing Key Laboratory of Printing and Packaging Materials and Technology, Beijing Institute of Graphic Communication, Beijing 102600, China; wujiao20220912@163.com (J.W.); drllqx@163.com (Q.L.); gaopeng08252022@163.com (P.G.)
[2] National Center for Nanoscience and Technology, CAS Key Laboratory of Nanophotonic Materials and Devices (Preparatory), Beijing 100190, China
[3] The GBA Research Innovation Institute for Nanotechnology, Guangzhou 510700, China
[4] Beijing Key Laboratory for Sensors, Beijing Information Science & Technology University, Beijing 100192, China; li@bistu.edu.cn
[5] CAS Center for Excellence in Nanoscience, Beijing Key Laboratory of Micro-Nano Energy and Sensor, Beijing Institute of Nanoenergy and Nanosystems, Chinese Academy of Sciences, Beijing 101400, China; jiangtao@binn.cas.cn
* Correspondence: jigangwang@bigc.edu.cn (J.W.); yuansheng-qi@bigc.edu.cn (Y.Q.); lizhenjun@nanoctr.cn (Z.L.)
† These authors contributed equally to this work.

Abstract: Herein, a series of novel long afterglow nanophosphors $BaYAl_3O_7:Eu^{2+}$, Nd^{3+} was synthesized by the combustion method. The investigation encompassed the characterization of X-ray diffraction, morphology, chemical valence, elemental composition, and photoluminescence behavior of $BaYAl_3O_7:Eu^{2+}$ and $BaYAl_3O_7:Eu^{2+}$, Nd^{3+} nanoparticles. Under 365 nm excitation, $BaYAl_3O_7:Eu^{2+}$ and $BaYAl_3O_7:Eu^{2+}$, Nd^{3+} show emission bands centered at 497 nm and 492 nm, which are attributed to the $4f^65d \rightarrow 4f^7$ transition of Eu^{2+} ions. The optimal samples of $BaYAl_3O_7:0.03Eu^{2+}$ and $BaYAl_3O_7:0.03Eu^{2+}$, $0.02Nd^{3+}$ have average fluorescence lifetimes of 850 ns and 1149 ns, respectively. The co-doping of Nd^{3+} ions as the trap centers produced long afterglow luminescence properties, and the afterglow time could reach up to 8 min. Furthermore, the fluorescent powder can be mixed with polyacrylic acid to prepare anti-counterfeiting inks; a clover pattern and snowflake pattern have been successfully printed using screen printing technology, proving its potential application in the field of anti-counterfeiting.

Keywords: long afterglow; $BaYAl_3O_7:Eu^{2+}$, Nd^{3+}; screen printing; anti-counterfeiting

1. Introduction

Long afterglow luminescent materials are a class of materials with special luminescent properties. The phosphors can absorb light energy for a short period and continue to emit light for a few seconds to a few days even after stopping external excitation [1,2]. First, because of their unique environmental protection, energy saving, and other characteristics, application potential of the materials is considered in lighting, security signs, night display, anti-counterfeiting, and other fields [3–8]. Second, long afterglow luminescent materials usually have tunable luminescent colors, which can be adjusted by adjusting the material composition, crystal structure, and doping ions to reach diverse luminescent effects. In addition, these materials usually have good chemical stability and optical properties and are suitable for use under various environmental conditions. Since 1996, when the first report appeared about the strong long afterglow luminescent materials $SrAl_2O_4:Eu^{2+}$,

Dy^{3+}, long afterglow rare-earth luminescent materials have been widely investigated. In $SrAl_2O_4:Eu^{2+}$, Dy^{3+} phosphor, Eu^{2+} serve as the luminescence center, while Dy^{3+} ions are thought to strongly enhance the sustained luminescence intensity [9,10].

Long afterglow luminescent materials often have two sorts of centers: emission centers and trap centers [11]. When stimulated by external energy, these emitting centers operate as photoactive centers, radiating in the visual range. Trap centers, on the other hand, which are accompanied by lattice defects, store energy and gradually release it to the emission centers once excitation has stopped. The color of the light emitted is usually determined by the emission center. As we all know, Eu^{2+} ions as efficient activators are common ions widely studied in the field of long afterglow materials [12–15]. In addition, to obtain or improve the long afterglow performance, one of the most common methods is by co-doping with RE^{3+} ions. It produces new traps or changes the inherent trap properties by non-equivalent substitution. In recent years, several remarkable long afterglow phosphors were developed using this strategy. For example, $CaAl_2O_4:Eu^{2+}$, Nd^{3+} (blue), $Sr_2MgSi_2O_7:Eu^{2+}$, Dy^{3+} (blue), $SrAl_2O_4:Eu^{2+}$, Dy^{3+} (green), $Ca_2BO_3Cl:Eu^{2+}$, Dy^{3+} (yellow), $Ca_3Si_2O_7:Eu^{2+}$, Sm^{3+}/Tm^{3+} (orange), $CaS:Eu^{2+}$, Tm^{3+} (red), $Sr_5(PO_4)_3Cl:Eu^{2+}$, Nd^{3+} (NIR) [9,16–21], etc. Furthermore, various synthetic processes, including sol-gel, combustion, and co-precipitation, have been used to synthesize these long afterglow luminescent materials [22–25]. Among these, the combustion method is simple to use, appropriate for high-volume and low-cost preparation, and permits the synthesis of nanoparticles with controlled shape and particle size at lower temperatures [11,26].

In this study, a novel $BaYAl_3O_7:Eu^{2+}$, Nd^{3+} long afterglow phosphor was prepared by the combustion method. Its photoluminescence (PL), optical band gap (E_g), thermoluminescence (TL), long afterglow properties, etc., were investigated. Then, the anti-counterfeiting inks were prepared, showing their potential applications in the field of anti-counterfeiting.

2. Experimental Section

2.1. Materials and Method

A series of $Ba_{0.5-0.5x-0.5y}Y_{0.5-0.5x-0.5y}Al_3O_7$: xEu^{2+}, yNd^{3+} (x = 0, 0.02, 0.03, 0.04, 0.05, 0.06; y = 0.01, 0.02, 0.03, 0.04, 0.05) samples was prepared by the combustion method. The raw materials used were $BaCO_3$ (purity: 99.99%), $Y(NO_3)_3$ (99.99%), Al_2O_3 (99.99%), Eu_2O_3 (99.99%), Nd_2O_3 (99.99%), HNO_3 (80%), and urea (99.99%), which were all purchased from Tianjin Chemical Reagent Factory. All reagents were directly used as received without further purification.

2.2. Synthesis of Nanomaterials

First, appropriate amounts of HNO_3 and deionized water were added to $BaCO_3$, $Y(NO_3)_3$, Al_2O_3, Eu_2O_3, and Nd_2O_3 to prepare 0.2 mmol/mL of $Ba(NO_3)_2$, 0.5 mmol/mL of $Y(NO_3)_3$, 1 mmol/mL of $Al(NO_3)_3$, 0.1 mmol/mL of $Eu(NO_3)_3$, and 0.5 mmol/mL of $Nd(NO_3)_3$ solutions, respectively. Then, $Ba(NO_3)_2$, $Y(NO_3)_3$, $Al(NO_3)_3$, $Eu(NO_3)_3$, and $Nd(NO_3)_3$ solutions were measured in stoichiometric ratios and placed in a crucible, then 2.2 g of urea for the combustion agent was added and mixed homogeneously, and placed in a muffle furnace preheated to 600 °C. After waiting for 3–5 min, a loose white and porous solid powder was obtained. Ultimately, the obtained samples were naturally cooled to room temperature and ground into powder for a test.

2.3. Preparation of Anti-Counterfeit Ink

The fluorescent powder was introduced into the mixture of ethanol and polyacrylic acid, where the volume ratio of fluorescent powder to the mixed solution was 3:1, followed by a long time of stirring. The amount of polyacrylic acid and ethanol is adjusted to achieve a suitable viscosity for screen printing to obtain the final fluorescent ink. Figure 1 provides a schematic diagram of the preparation of phosphors and screen printing.

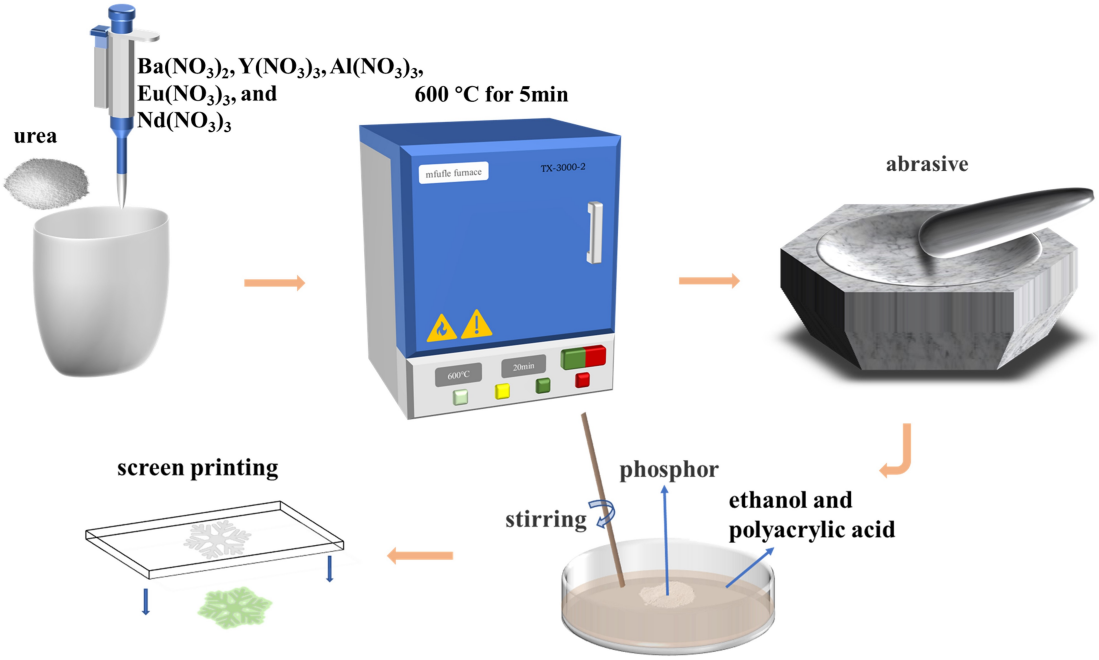

Figure 1. Schematic diagram of ink preparation and screen printing.

2.4. Characterizations

The crystalline phases were determined by X-ray diffraction (D/Max-2400 by Rigaku, Tokyo, Japan) analysis with Cu Kα radiation (λ = 1.54 Å). The binding energy was obtained with x-ray photoelectron spectroscopy (XPS, Thermo Fisher Scientific ESCALAB 250 XI, Waltham, MA, USA). The photoluminescence excitation (PLE) and PL spectra were measured by a fluorescence spectrometer (FluoroMax-4, F4700, Hitachi, Tokyo, Japan) equipped with a Xe lamp. The morphology of phosphors was observed through scanning electron microscopy (Quanta 250 FEG, Hitachi, Tokyo, Japan). The sample's luminescence was measured with a UV lamp supplied by HUNNENGSHI. The fluorescence lifetime and afterglow decay curves of phosphors were measured by a transient steady-state fluorescence spectrometer (FLS1000, Edinburgh Instruments, Edinburgh, UK). The UV-Vis absorption spectra were obtained using a UV-3600 UV-Vis Near Infrared Spectrophotometer (Shimadzu Corporation, Kyoto, Japan). The energy-dispersive X-ray spectroscopy (EDS, SU8020, Hitachi, Tokyo, Japan) spectrum was obtained with a desktop scanning electron microscope energy dispersive spectrometer (Phenom Pro X, Thermo Fisher Scientific, Landsmeer, The Netherlands). The TL was tested with a thermal spectrometer (FJ-427A, China National Nuclear Corporation, Tianjin, China) at a heating rate of 1 °C/s.

3. Results and Discussion

3.1. XRD Patterns and Morphology Analysis

The X-ray diffraction (XRD) patterns of $BaYAl_3O_7$:xEu^{2+}(x = 0, 0.02, 0.03, 0.04, 0.05, 0.08) nanophosphors obtained by calcining at 600 °C are presented in Figure 2a. The information regarding $BaYAl_3O_7$ (abbreviated as BYAO) is not found in the present literature. Figure 2a exhibits the XRD patterns of the BYAO hosts, doped BYAO samples, and standard cards of the $BaAl_2O_4$ (PDF#00-017-0306) and $Y_3Al_5O_{12}$ (PDF#01-073-1370) [27,28]. It is observed that the sample has a mixture phase structure and the diffraction peaks match well with the standard cards of the $BaAl_2O_4$ and $Y_3Al_5O_{12}$. Generally, it is reasonable to assume that the Eu^{2+} dopants tend to occupy the Ba^{2+}/Y^{3+} sites based on similar effective ionic radii (IR) of the cation with varying coordination numbers (CNs) [29–31]. Moreover, the main diffraction peak shifts toward a higher angle with the introduction of Eu ions, as shown in Figure 2a. It implies that the replaced sample lattice characteristics and cell volume are lowered to some amount, which is consistent with the shift of diffraction peaks,

which might be well-accepted based on Bragg's law ($2d \sin\theta = n\lambda$) [32,33]. It verifies once more that Eu ions with lower ionic radii are continually replacing potentially substitutable ions. The XRD patterns of the $BaYAl_3O_7$:0.03Eu^{2+}, xNd^{3+} (x = 0.01, 0.02, 0.03, 0.04, 0.05) nanophosphors obtained by the calcination at 600 °C are presented in Figure 2b. Compared with Figure 2a, the positions of the diffraction peaks remain basically the same, which indicates that the co-doping of Nd^{3+} ions does not change the crystal phase of the BYAO host. Based on the consideration of the effective ionic radii with different coordination numbers [34], the co-doped rare-earth ion Nd^{3+} is proposed to occupy the Ba^{2+}/Y^{3+} site in the main lattice of the BAYO.

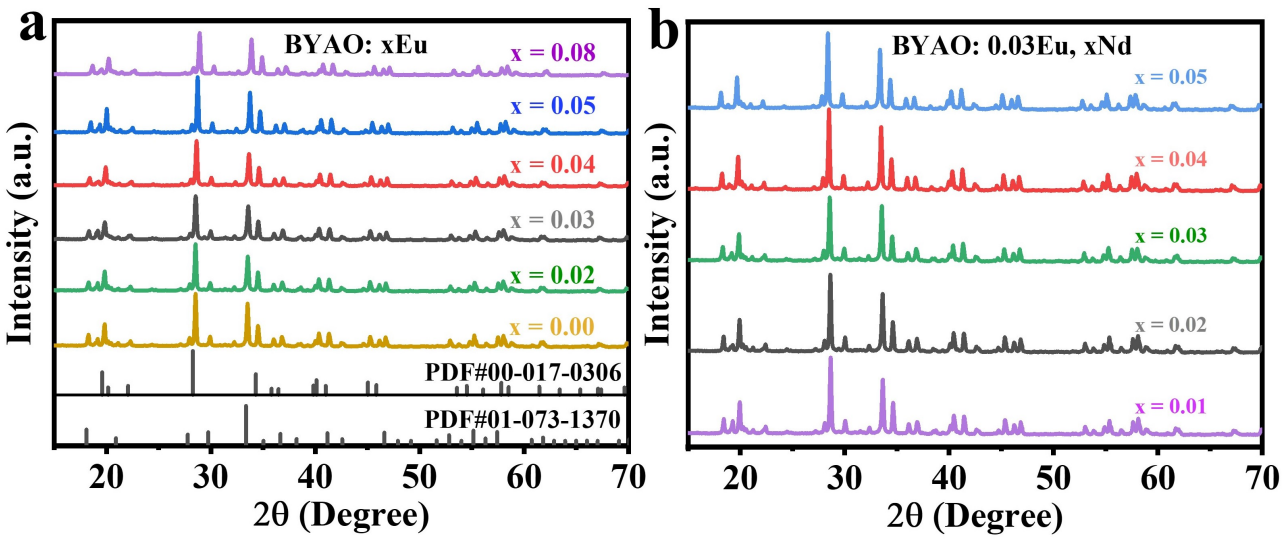

Figure 2. (**a**) The BYAO:xEu^{2+} (x = 0, 0.02, 0.03, 0.04, 0.05, 0.08) XRD patterns and the standard card. (**b**) The XRD patterns of $BaYAl_3O_7$:0.03 Eu^{2+}, xNd^{3+} (x = 0.01, 0.02, 0.03, 0.04, 0.05) phosphors.

Since the chemical valence of Eu and Nd can greatly affect the luminescence performance, it is crucial to determine the valence states of the Eu and Nd ions in the BYAO host. The valence states of Eu and Nd were studied using XPS. As shown in Figure 3, the XPS measurements exhibit binding energies corresponding to Ba 3d, Y 3d, Al 2p, O 1s, Eu 3d, and Nd 3d [35–37]. Furthermore, as shown in Figure 3e, the high-resolution (HR) XPS depicts the binding energy of the Eu 3d (1125.09 eV) signal, which is consistent with that of Eu^{2+} $3d_{5/2}$ [38–40]. The binding energy of Nd 3d peaks at 977.2 eV (Nd $3d_{5/2}$) and 1000.6 eV (Nd $3d_{3/2}$) as can be seen in Figure 3f [41–46]. Figures 4a and 5a show scanning electron microscopy (SEM) pictures of the BYAO:0.03Eu^{2+} and BYAO:0.03Eu^{2+}, 0.02Nd^{3+}. The irregularities in the shape, size, and pores of these samples may be related to the irregular mass flow and inhomogeneous temperature distribution of the samples during combustion [47]. The EDS of the BYAO:0.03Eu^{2+} and BYAO:0.03Eu^{2+}, 0.02Nd^{3+} phosphors is displayed in Figures 4b and 5b, and the EDS intensity signals of Ba, Y, Al, O, Eu, and Nd are in good agreement with the chemical composition of the BYAO:0.03Eu^{2+} and BYAO:0.03Eu^{2+}, 0.02Nd^{3+} phosphors. Moreover, from the mapping analysis in Figures 4c and 5c, it is clearly observed that Eu and Nd are uniformly distributed over the BYAO host.

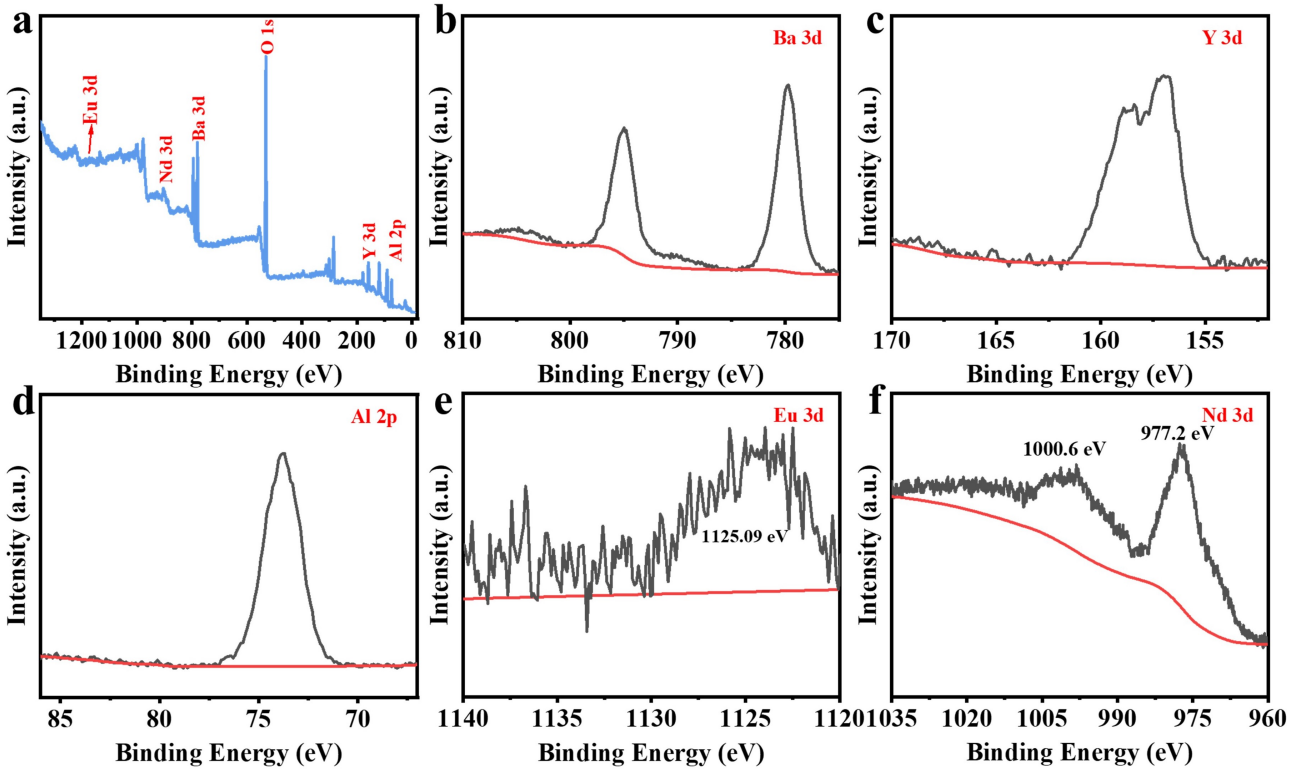

Figure 3. (**a**) The XPS spectra of the BYAO:0.03 Eu^{2+}, 0.02 Nd^{3+}. (**b**–**f**) The HR XPS spectra of Ba 3d, Y 3d, Al 2p, Eu 3d, and Nd 3d.

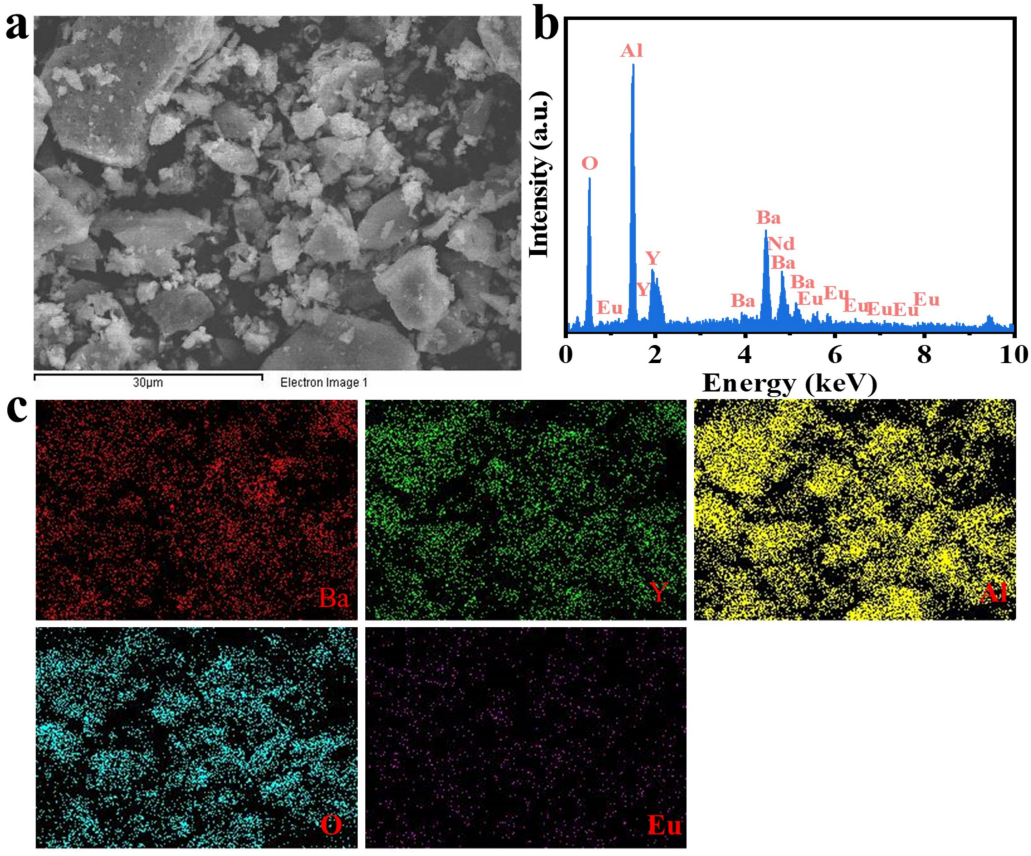

Figure 4. (**a**) The SEM image of the BYAO:0.03Eu^{2+} material. (**b**) The EDS of the BYAO:0.03Eu^{2+} material. (**c**) The elemental distribution of the BYAO:Eu^{2+} material.

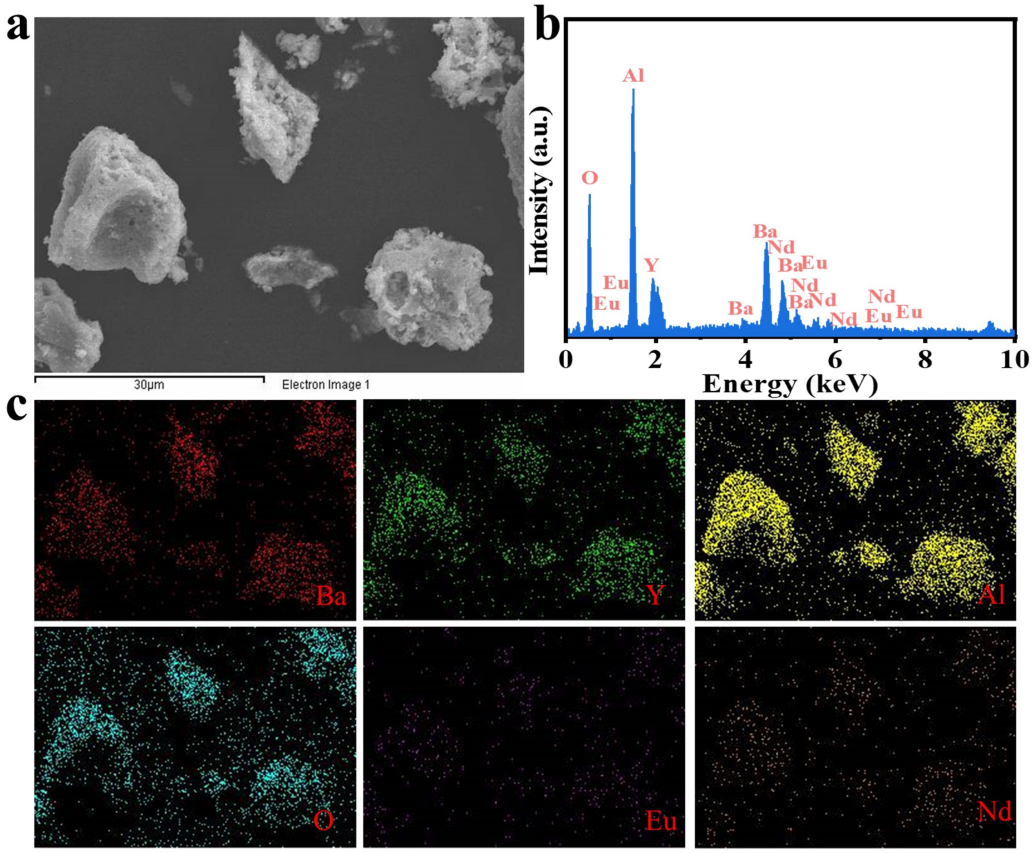

Figure 5. (**a**) The SEM image of the BYAO:0.03Eu^{2+}, 0.02Nd^{3+} material. (**b**) The EDS of the BYAO:0.03Eu^{2+}, 0.02Nd^{3+} material. (**c**) The elemental distribution of the BYAO:0.03Eu^{2+}, 0.02Nd^{3+} material.

3.2. Photoluminescence and Afterglow Properties

Figure 6a,b display the UV–vis absorption spectra of the BYAO:0.03Eu^{2+} and BYAO:0.03Eu^{2+}, 0.02Nd^{3+}. The bandgap (E_g) can be calculated on the basis of the following equation:

$$(\alpha h\nu)^2 = A(h\nu - E_g) \quad (1)$$

$h\nu$ is the photon energy, α is the absorption coefficient, E_g is band gap energy (eV), and A is a constant [40,48,49]. The insets show the experimental values (E_g), which are approximately 4.92 eV and 5.26 eV. The optical properties of the BYAO:Eu^{2+} and BYAO:Eu^{2+}, Nd^{3+} phosphors were analyzed by analyzing PLE and PL spectra. As shown in Figure 6c, the PLE spectrum of BYAO:Eu^{2+}, Nd^{3+} shows a broad absorption band centered at 365 nm, which is mainly due to the $4f^7 \rightarrow 4f^6 5d$ transition of Eu^{2+} ions [50–53]. Under the 365 nm UV light excitation, the PL spectrum of the BYAO:0.03Eu^{2+} (~497 nm) and BYAO:0.03Eu^{2+}, 0.02Nd^{3+} (~492 nm) shows the $4f^6 5d \rightarrow 4f^7$ transitions of Eu^{2+} ions [53–55]. Because of the relatively small crystal-field splitting energy for Eu^{2+} ions in the BYAO host crystal, the light emission from the BYAO:Eu^{2+} and BYAO:Eu^{2+}, Nd^{3+} phosphors is considerably shorter wavelength, peaking at ~500 nm, than the various Eu^{2+}-doped phosphors [53]. The intensity of the Eu^{2+} single-doped sample is higher than that of the Eu^{2+}, Nd^{3+} co-doped samples, and the emission spectrum is slightly blue-shifted after co-doping, indicating that there may be energy storage in the co-doped samples during this process [13]. Furthermore, in the Eu^{2+}, Nd^{3+} co-doped samples, no emission characteristics of Nd^{3+} ions were observed, suggesting that Nd^{3+} is not acting as a luminescence center but may play the role of a trapping center. To investigate the doping concentration effect on the optical properties of the samples, BYAO:xEu^{2+} (x = 0, 0.02, 0.03, 0.04, 0.05, 0.08) phosphors were synthesized. In Figure 7a, under the excitation of 365 nm, the PL spectra of the phosphors doped with different concentrations of Eu^{2+} show that the optimum concentration is 0.03Eu^{2+}. The

luminescence intensity is an increase of 29 times the original intensity. To further investigate the effect of Nd^{3+} concentration, the typical experiment was performed for BYAO:0.03Eu^{2+}, xNd^{3+} (x = 0.01–0.05). As seen in Figure 7b, the emission intensity reaches its highest when the doping concentration is 0.02. Figure 7c depicts the coherent infrared energy (CIE) chromaticity coordinate positions of the BYAO:0.03Eu^{2+}, xNd^{3+} (0–0.05) phosphors under the excitation wavelength of 365 nm. With the increased Nd ion concentration, the emission color gradually blue-shifted, and the corresponding CIE color coordinates are changed from (0.151, 0.0.305) to (0.148, 0.216).

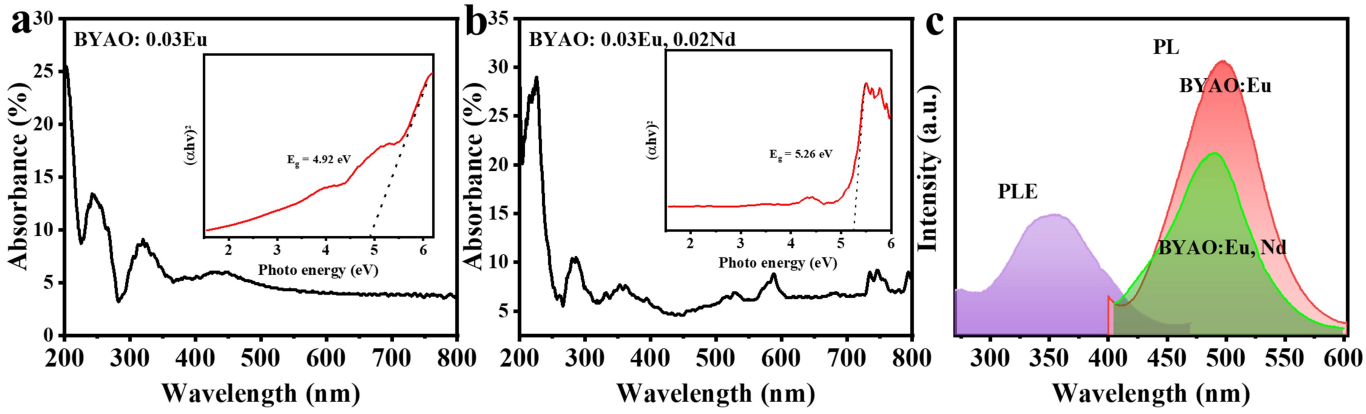

Figure 6. (**a**,**b**) UV–vis absorption spectrum of the BYAO:0.03Eu^{2+} and BYAO:0.03Eu^{2+}, 0.02Nd^{3+}. The inset shows the theoretical fit of the band gap. (**c**) The emission spectra (λ_{ex} = 365 nm) and excitation spectra (λ_{em} = 496 nm) of the samples.

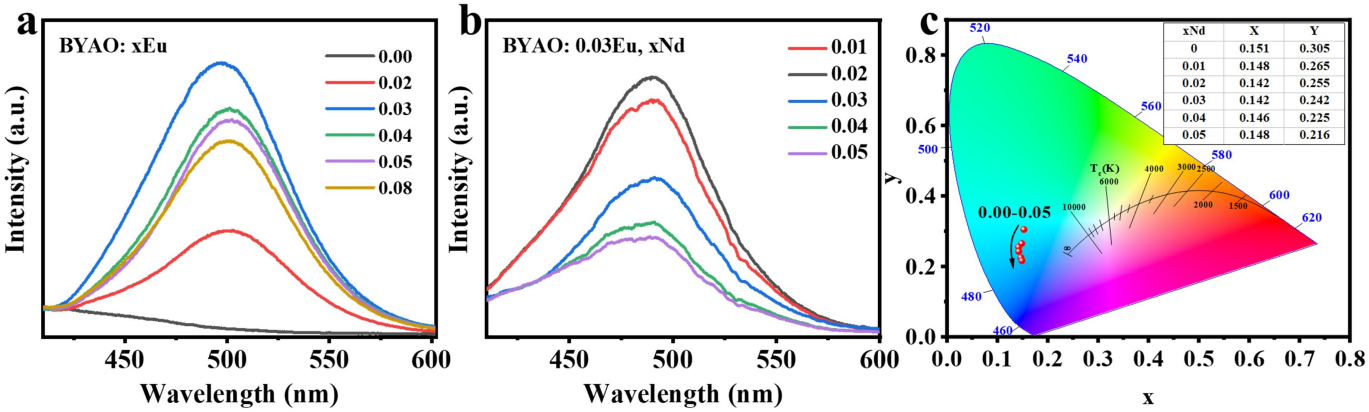

Figure 7. (**a**,**b**) The emission spectra (λ_{ex} = 365 nm) of the BYAO:xEu^{2+} (x = 0, 0.02, 0.03, 0.04, 0.05, 0.08) and BYAO:0.03Eu^{2+}, xNd^{3+} (x = 0.01, 0.02, 0.03, 0.04, 0.05). (**c**) CIE chromaticity diagram of the BYAO:0.03Eu^{2+}, xNd^{3+} (0–0.05) under the excitation of 365 nm ultraviolet light.

In addition, Figure 8a shows the luminescence decay curves of BYAO:0.03Eu^{2+} and BYAO:0.03Eu^{2+}, 0.02Nd^{3+} phosphors (λ_{ex} = 365 nm). The decay curve can be well-fitted with a second-order exponential function [56]:

$$I(t) = I_0 + A_1 exp(-t/\tau_1) + A_2 exp(-t/\tau_2)) \quad (2)$$

where I_0 represents the background constant, A_1 and A_2 are constants, and τ_1 and τ_2 represent the decay times for the fast and slow exponential components, respectively. The average decay time τ^* could be obtained using the following equation:

$$\tau^* = (A_1 \cdot \tau_1^2 + A_2 \cdot \tau_2^2)/(A_1 \cdot \tau_1 + A_2 \cdot \tau_2) \quad (3)$$

The average decay time τ^* of the BYAO:0.03Eu^{2+} and BYAO:0.03Eu^{2+}, 0.02Nd^{3+} phosphors is 850 ns and 1149 ns, respectively, which provides experimental evidence for the presence of an energy transfer process between Eu^{2+} ions and Nd^{3+} ions [57]. To further investigate the afterglow properties of phosphors, the afterglow decay curve of the BYAO:0.03Eu^{2+}, 0.02Nd^{3+} samples was measured. As shown in Figures 8b and 9, a bright blue-green afterglow can be observed after exposing the BYAO:0.03Eu^{2+}, 0.02Nd^{3+} phosphor to a 365 UV light for 5 min, and the afterglow time is more than 8 min, which shows the potential application as a nighttime security marker. The afterglow curve can be fitted by the double-exponential Equation (2). According to the above equation, τ_1 and τ_2 are 5.4 s and 51.3 s, respectively. Long afterglow decay occurs in two stages: slow decay and quick decay. These quick decay processes appear first and dominate the intensity. Slow decay processes take place later and result in long-term luminescence behavior [58,59].

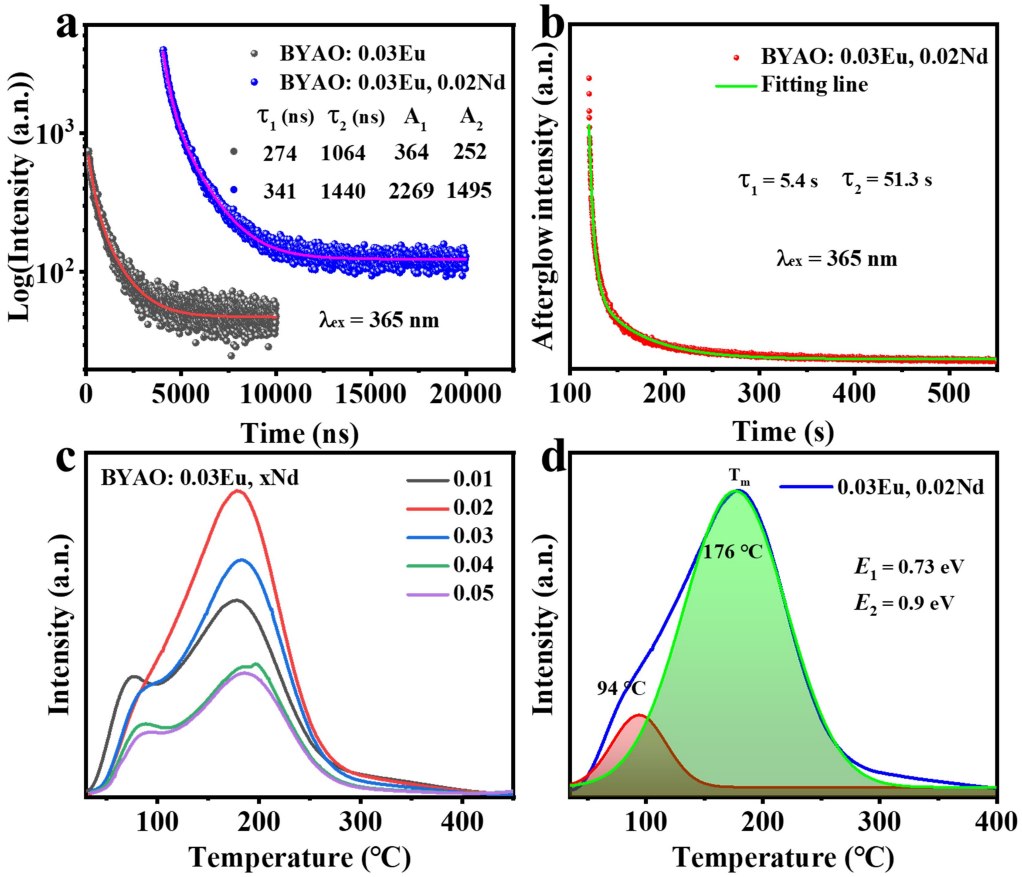

Figure 8. (**a**) The luminescence decay curves of the BYAO:0.03Eu^{2+} and BYAO:0.03Eu^{2+}, 0.02Nd^{3+} phosphors. (**b**) Afterglow decay curve of the BYAO:0.03Eu^{2+}, 0.02Nd^{3+} phosphor after exposure to a 365 nm UV light for 2 min. (**c**) Concentration-dependent TL curves of the BYAO:0.03Eu^{2+}, xNd^{3+} (x = 0.01–0.05) excited for 5 min. (**d**) TL spectrum of the BYAO:0.03Eu^{2+}, 0.02Nd^{3+} and its deconvolution into the two Gaussian components at 94 and 176 °C.

The long afterglow is a result of the gradual release of charge carriers trapped in the material, with the afterglow duration and intensity depending on the concentration and depth of the trapping centers. Shallow traps are adversely affected by stable charge carriers, significantly reducing the duration of persistent luminescence. Conversely, charge carriers captured by deep traps are difficult to release at room temperature, also adversely impacting the persistence of luminescence [2]. Therefore, to investigate the afterglow process in detail, the trap information of the BYAO:0.03Eu^{2+}, xNd^{3+} (x = 0.01–0.05) samples was analyzed using TL spectra, as shown in Figure 8c. The samples were exposed to 365 nm UV light pre-irradiation for 5 min at room temperature (30 °C), heating to 500 °C,

quickly cooling to 30 °C, and final TL measurement at a heating rate of 1 °C/s. With the increase in the concentration of Nd ions, the high-temperature peak gradually shifts to higher temperatures, which means that the doping of Nd^{3+} ions significantly increases the defect levels. As shown in Figure 8d, the TL curve of BYAO:0.03Eu^{2+}, 0.02Nd^{3+} consists of two broad bands with maxima at 94 °C and 176 °C, which correspond to the shallow and deep traps, respectively. The depth of the trap can be estimated by the following equation [60–62]:

$$E = \frac{T_m}{500} \quad (4)$$

where E represents the activation energy (depth of the trap), T_m represents the peak temperature: for the shallow trap, T_m = 94 °C; for the deep trap, T_m = 176 °C. Therefore, the depths of the deep and shallow traps in BYAO:0.03Eu^{2+}, 0.02Nd^{3+} are evaluated to be 0.73 eV and 0.9 eV, respectively.

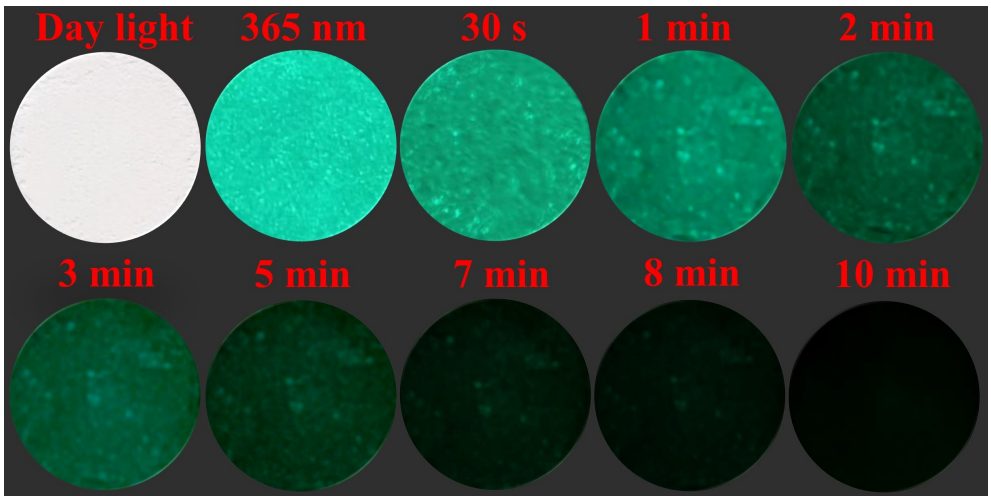

Figure 9. Afterglow photographs of BYAO:0.03Eu^{2+}, 0.02Nd^{3+} phosphor after exposure to the 365 nm UV source for 5 min.

3.3. Mechanism for the Afterglow of the BYAO:Eu^{2+}, Nd^{3+} Phosphor

When Nd^{3+} ions replace Ba^{2+} ions in the matrix, a positive charge center is generated due to the need to maintain charge balance, that is, a trap is created. Figure 10 shows the possible mechanism for the formation of efficient blue-green afterglow in Eu^{2+}, Nd^{3+} co-doped BYAO. When the UV photon excites a sample, electrons are excited from the ground state to the excited state or conduction band (CB). The excited electrons will transit back to the ground state and recombine with holes to emit light. The electrons in the CB will become free electrons, and after the light irradiation stops, the free electrons in the CB will partly relax to the excited state and subsequently transit back to the ground state and recombine with holes to luminesce. Another part of the free electrons in the CB will be captured by the shallow and deep traps. The electrons that enter the shallow trap slowly escape due to thermal excitation and relax to the CB. Relaxation to the CB of part of the free electrons by the trap then occurs, and they are then captured, and part of the free electron relaxation to the excited state takes place, whereupon they transition back to the ground state and recombine with holes, resulting in afterglow luminescence. Electrons in deep traps also slowly escape and relax into shallow traps due to thermal excitation. The electrons captured in the deep traps do not escape directly into the CB at room temperature, and so the deep trap has a storage function.

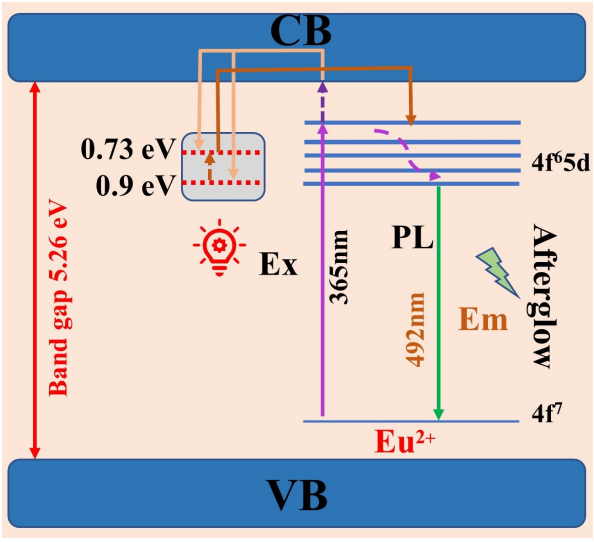

Figure 10. Schematic afterglow mechanism in the BYAO:Eu^{2+}, Nd^{3+} phosphor.

3.4. Anti-Counterfeiting Application

To further investigate the anti-counterfeiting properties of phosphor, we prepared anti-counterfeiting inks by mixing phosphor with polyacrylic acid and then printed four-leaf clover and snowflake patterns with the screen printing technique. As shown in Figure 11a,b, BYAO/ink is almost invisible under daylight, and clear patterns can be seen under the 365 nm UV excitation. As shown in Figure 11c,d, the pattern printed by BYAO:0.03Eu^{2+}, 0.02Nd^{3+}/ink can still be seen clearly after the UV irradiation is turned off. In addition, the afterglow effect can still be seen after the UV excitation has stopped for three minutes. From the above findings, we suggested that the Eu^{2+} ions and Nd^{3+} ions activating the BYAO ink are anticipated for high-level anti-counterfeiting applications.

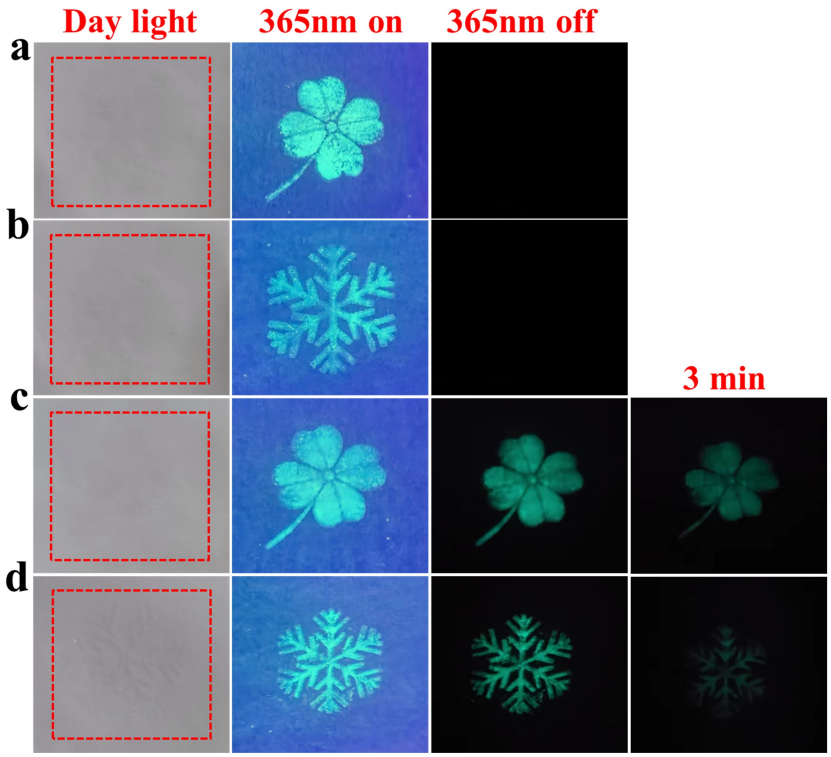

Figure 11. BYAO:0.03Eu^{3+}/ink for printing (**a**) four-leaf clover and (**b**) snowflake patterns; BYAO:0.03Eu^{2+}, 0.02Nd^{3+}/ink for printing (**c**) four-leaf clover and (**d**) snowflake patterns.

4. Conclusions

In summary, a series of BYAO:Eu^{2+} and BYAO:Eu^{2+}, Nd^{3+} phosphors was prepared via the combustion method at a reaction temperature of 600 °C. The Eu^{2+} ions and Nd^{3+} ions were successfully doped into the BYAO host, as was verified by XRD, EDS, and XPS analysis. The emission bands of BYAO:Eu^{2+} and BYAO:Eu^{2+}, Nd^{3+} are centered at 497 and 492 nm, respectively, which are attributed to the $4f^65d \rightarrow 4f^7$ transition of Eu^{2+} ions. The fluorescence lifetimes of the BYAO:0.03Eu^{2+} and BYAO:0.03Eu^{2+}, 0.02Nd^{3+} are 850 ns and 1149 ns, respectively. In addition, Eu^{2+} ions as the emission center and co-doped Nd^{3+} ions as the trap center can improve the afterglow performance. The afterglow duration of the BYAO:0.03Eu^{2+}, 0.02Nd^{3+} phosphor can reach 8 min. Finally, a transparent ink was prepared by mixing fluorescent powder with ethanol and polyacrylic acid to demonstrate the potential of fluorescent powder for anti-counterfeiting applications.

Author Contributions: J.W. (Jiao Wu), Q.L. and P.G. designed and carried out the experiment. J.W. (Jiao Wu), J.W. (Jigang Wang), and T.J. processed the test data. With the help of Y.Q., Z.L., and J.L. wrote and completed the paper. All authors have read and agreed to the published version of the manuscript.

Funding: This research is supported by Beijing Natural Science Foundation (No. 2202018), the General Project of Beijing Municipal Education Commission Science and Technology Program (No. KM202010015004), the Research and development of intelligent packaging for cultural relics (Ed202001), the Construction and application transformation of cross media cloud platform for printing and packaging anticounterfeiting and traceability (27170121005), the National Natural Science Foundation of China (No. 21604005, Grant No. 52072084), the general project of fundamental research of BIGC (No. Ed202208, Eb202001, 20190122041, 22150122042, 22150122034, 27170122012), the Initial funding for the Doctoral Program of BIGC (No. 27170121001/002), and the general project of science and technology of Beijing Municipal Education Commission (No. KM202110015008), the Key Area Research and Development Program of Guangdong Province (Grant no. 2020B0101020002), the GBA National Institute for Nanotechnology Innovation (Grant No. 2020GN0106), the National Key R&D Program of China (Grant No. 2021YFC2802000), the National key research and development program (2019YFB1707202).

Data Availability Statement: Research data are not shared.

Conflicts of Interest: The authors declare no conflict of interest.

References

1. Pan, Z.; Lu, Y.Y.; Liu, F. Sunlight-activated long-persistent luminescence in the near-infrared from Cr^{3+}-doped zinc gallogermanates. *Nat. Mater.* **2012**, *11*, 58–63. [CrossRef] [PubMed]
2. Vaidyanathan, S. Recent Progress on Lanthanide-based Long Persistent Phosphors: An Overview. *J. Mater. Chem. C* **2023**, *11*, 8649–8687. [CrossRef]
3. Wang, J.; Su, Q.; Wang, S. Blue and red long lasting phosphorescence (LLP) in β-$Zn_3(PO_4)_2$:Mn^{2+}, Zr^{4+}. *J. Phys. Chem. Solids* **2005**, *66*, 1171–1176. [CrossRef]
4. Liang, L.; Chen, N.; Jia, Y.; Ma, Q.; Wang, J.; Yuan, Q.; Tan, W. Recent progress in engineering near-infrared persistent luminescence nanoprobes for time-resolved biosensing/bioimaging. *Nano Res.* **2019**, *12*, 1279–1292. [CrossRef]
5. Li, H.; Pang, R.; Sun, W.; Li, H.; Ma, T.; Jia, Y.; Li, D.; Jiang, L.; Zhang, S.; Li, C. $Sr_{1.7}Zn_{0.3}CeO_4F_{0.2}$:$Eu^{3+}$: Novel dual-emission temperature sensors for remote, noncontact thermometric application. *RSC Adv.* **2017**, *7*, 9645–9652. [CrossRef]
6. Poelman, D.; Van der Heggen, D.; Du, J.; Cosaert, E.; Smet, P.F. Persistent phosphors for the future: Fit for the right application. *J. Appl. Phys.* **2020**, *128*, 240903. [CrossRef]
7. Gupta, I.; Singh, S.; Bhagwan, S.; Singh, D. Rare earth (RE) doped phosphors and their emerging applications: A review. *Ceram. Int.* **2021**, *47*, 19282–19303. [CrossRef]
8. Lian, S.; Qi, Y.; Rong, C.; Yu, L.; Zhu, A.; Yin, D.; Liu, S. Effectively leveraging solar energy through persistent dual red phosphorescence: Preparation, characterization, and density functional theory study of $Ca_2Zn_4Ti_{16}O_{38}$:Pr^{3+}. *J. Phys. Chem. C* **2010**, *114*, 7196–7204. [CrossRef]
9. Matsuzawa, T.; Aoki, Y.; Takeuchi, N.; Murayama, Y. A new long phosphorescent phosphor with high brightness, $SrAl_2O_4$:Eu^{2+}, Dy^{3+}. *J. Electrochem. Soc.* **1996**, *143*, 2670. [CrossRef]
10. Kong, J.; Meijerink, A. Identification and Quantification of Charge Transfer in $CaAl_2O_4$:Eu^{2+}, Nd^{3+} Persistent Phosphor. *Adv. Opt. Mater.* **2023**, p. 2203004. [CrossRef]

11. Kadyan, S.; Singh, S.; Simantilleke, A.P.; Singh, D. Synthesis and optical studies of nanocrystalline Eu^{2+}-doped and RE^{3+} (Nd^{3+}, Dy^{3+})-codoped $Ba_4Al_{14}O_{25}$ materials for UV-LEDs. *Optik* **2020**, *212*, 164671. [CrossRef]
12. Palilla, F.C.; Levine, A.K.; Tomkus, M.R. Fluorescent properties of alkaline earth aluminates of the type MAl_2O_4 activated by divalent europium. *J. Electrochem. Soc.* **1968**, *115*, 642. [CrossRef]
13. Zeng, W.; Wang, Y.; Han, S.; Chen, W.; Li, G. Investigation on long-persistent luminescence of $Ca_2BO_3Cl:Eu^{2+}$, Ln^{3+} (Ln = Nd, Dy, Er). *Opt. Mater.* **2014**, *36*, 1819–1821. [CrossRef]
14. Yang, Y.M.; Li, Z.Y.; Zhang, J.Y.; Lu, Y.; Guo, S.Q.; Zhao, Q.; Wang, X.; Yong, Z.J.; Li, H.; Ma, J.P.; et al. X-ray-activated long persistent phosphors featuring strong UVC afterglow emissions. *Light. Sci. Appl.* **2018**, *7*, 88. [CrossRef] [PubMed]
15. Zhuang, Y.; Lv, Y.; Li, Y.; Zhou, T.; Xu, J.; Ueda, J.; Tanabe, S.; Xie, R.J. Study on trap levels in $SrSi_2AlO_2N_3:Eu^{2+}$, Ln^{3+} persistent phosphors based on host-referred binding energy scheme and thermoluminescence analysis. *Inorg. Chem.* **2016**, *55*, 11890–11897. [CrossRef] [PubMed]
16. Yamamoto, H.; Matsuzawa, T. Mechanism of long phosphorescence of $SrAl_2O_4:Eu^{2+}$, Dy^{3+} and $CaAl_2O_4:Eu^{2+}$, Nd^{3+}. *J. Lumin.* **1997**, *72*, 287–289. [CrossRef]
17. Lin, Y.; Tang, Z.; Zhang, Z.; Wang, X.; Zhang, J. Preparation of a new long afterglow blue-emitting $Sr_2MgSi_2O_7$-based photoluminescent phosphor. *J. Mater. Sci. Lett.* **2001**, *20*, 1505–1506. [CrossRef]
18. Zeng, W.; Wang, Y.; Han, S.; Chen, W.; Li, G.; Wang, Y.; Wen, Y. Design, synthesis and characterization of a novel yellow long-persistent phosphor:$Ca_2BO_3Cl:Eu^{2+}$, Dy^{3+}. *J. Mater. Chem. C* **2013**, *1*, 3004–3011. [CrossRef]
19. Ueda, J.; Maki, R.; Tanabe, S. Vacuum referred binding energy (VRBE)-guided design of orange persistent $Ca_3Si_2O_7:Eu^{2+}$ phosphors. *Inorg. Chem.* **2017**, *56*, 10353–10360. [CrossRef]
20. Suda, Y.; Tamura, Y.; Yamaguchi, S.; Nanai, Y.; Okuno, T. Red afterglow and luminescence arising from defects in $CaS:Eu^{2+}$, Tm^{3+}. *J. Phys. D Appl. Phys.* **2021**, *54*, 415103. [CrossRef]
21. Talewar, R.A.; Mahamuda, S.; Rao, A.; Gaikwad, V.M.; Belsare, P.; Moharil, S. Broadband excited Nd^{3+} NIR emission in $Sr_5(PO_4)_3Cl:Eu^{2+}$, Nd^{3+} phosphor for solar spectral modification. *J. Lumin.* **2020**, *222*, 117118. [CrossRef]
22. Peng, T.; Huajun, L.; Yang, H.; Yan, C. Synthesis of $SrAl_2O_4$:Eu, Dy phosphor nanometer powders by sol–gel processes and its optical properties. *Mater. Chem. Phys.* **2004**, *85*, 68–72. [CrossRef]
23. Zand, S.K.; Baghshahi, S.; Rajabi, M. The effect of Eu and Dy dopants on the luminescence properties of $Sr_4Al_{14}O_{25}:Eu^{2+}$, Dy^{3+} phosphorescent nano-pigments prepared by the solution combustion method. *J. Mater. Sci. Mater. Electron.* **2016**, *27*, 12533–12538. [CrossRef]
24. Nikhare, G.; Gedam, S.; Dhoble, S. Luminescence in $Sr_4Al_{14}O_{25}:Ce^{3+}$ aluminate phosphor. *Luminescence* **2015**, *30*, 163–167. [CrossRef] [PubMed]
25. Chang, C.; Yuan, Z.; Mao, D. Eu^{2+} activated long persistent strontium aluminate nano scaled phosphor prepared by precipitation method. *J. Alloys Compd.* **2006**, *415*, 220–224. [CrossRef]
26. Panasyuk, G.; Kozerozhets, I.; Semenov, E.; Azarova, L.; Belan, V.; Danchevskaya, M. A New Method for producing a nanosized γ-Al_2O_3 powder. *Russ. J. Inorg. Chem.* **2018**, *63*, 1303–1308. [CrossRef]
27. Rafiaei, S.M.; Dini, G.; Bahrami, A. Synthesis, crystal structure, optical and adsorption properties of $BaAl_2O_4:Eu^{2+}$, Eu^{2+} / L^{3+} (L = Dy, Er, Sm, Gd, Nd, and Pr) phosphors. *Ceram. Int.* **2020**, *46*, 20243–20250. [CrossRef]
28. Singh, S.; Gupta, I.; Singh, D. Sm^{3+}-activated YAG nanocrystals: Synthesis, structural and spectroscopic analysis for orange-red emitting LEDs. *Optik* **2021**, *238*, 166482. [CrossRef]
29. Zheng, B.; Fan, J.; Chen, B.; Qin, X.; Wang, J.; Wang, F.; Deng, R.; Liu, X. Rare-earth doping in nanostructured inorganic materials. *Chem. Rev.* **2022**, *122*, 5519–5603. [CrossRef]
30. Wang, Y.; Seto, T.; Ishigaki, K.; Uwatoko, Y.; Xiao, G.; Zou, B.; Li, G.; Tang, Z.; Li, Z.; Wang, Y. Pressure-Driven Eu^{2+}-Doped $BaLi_2Al_2Si_2N_6$: A New Color Tunable Narrow-Band Emission Phosphor for Spectroscopy and Pressure Sensor Applications. *Adv. Funct. Mater.* **2020**, *30*, 2001384. [CrossRef]
31. Shannon, R.D. Revised effective ionic radii and systematic studies of interatomic distances in halides and chalcogenides. *Acta Crystallogr. Sect. A Cryst. Phys. Diffr. Theor. Gen. Crystallogr.* **1976**, *32*, 751–767. [CrossRef]
32. Wang, H.; Li, Z.; Kang, R.; Ji, R.; Wang, Y. $Sr_2BN_2Cl:Eu^{2+}$-Based Narrow-Band Blue-Emitting Phosphor: A Potential Color Converter for Illumination and Displays. *Inorg. Chem.* **2022**, *61*, 18245–18252. [CrossRef] [PubMed]
33. Li, J.; Liu, J.; Ni, Q.; Zhu, Q.; Zeng, Z.; Huo, J.; Long, C.; Wang, Q. Key Role Effect of Samarium in Realizing Zero Thermal Quenching and Achieving a Moisture-Resistant Reddish-Orange Emission in $Ba_3LaNb_3O_{12}:Sm^{3+}$. *Inorg. Chem.* **2022**, *61*, 17883–17892. [CrossRef] [PubMed]
34. Brgoch, J.; Hasz, K.; Denault, K.A.; Borg, C.K.; Mikhailovsky, A.A.; Seshadri, R. Data-driven discovery of energy materials: Efficient $BaM_2Si_3O_{10}:Eu^{2+}$ (M = Sc, Lu) phosphors for application in solid state white lighting. *Faraday Discuss.* **2014**, *176*, 333–347. [CrossRef] [PubMed]
35. Atuchin, V.; Kesler, V.; Kokh, A.; Pokrovsky, L. X-ray photoelectron spectroscopy study of β-BaB_2O_4 optical surface. *Appl. Surf. Sci.* **2004**, *223*, 352–360. [CrossRef]
36. Rubio, E.; Atuchin, V.; Kruchinin, V.; Pokrovsky, L.; Prosvirin, I.; Ramana, C. Electronic structure and optical quality of nanocrystalline Y_2O_3 film surfaces and interfaces on silicon. *J. Phys. Chem. C* **2014**, *118*, 13644–13651. [CrossRef]
37. Atuchin, V.V.; Vinnik, D.; Gavrilova, T.; Gudkova, S.; Isaenko, L.; Jiang, X.; Pokrovsky, L.; Prosvirin, I.; Mashkovtseva, L.; Lin, Z. Flux crystal growth and the electronic structure of $BaFe_{12}O_{19}$ hexaferrite. *J. Phys. Chem. C* **2016**, *120*, 5114–5123. [CrossRef]

38. Dong, C.; Zhang, Y.; Duan, J.; Yu, J. Synthesis and luminescence properties of single-phase $Ca_2P_2O_7$:Eu^{2+}, Eu^{3+} phosphor with tunable red/blue emission. *J. Mater. Sci. Mater. Electron.* **2019**, *30*, 16384–16394. [CrossRef]
39. Chae, K.W.; Park, T.R.; Cheon, C.I.; Cho, N.I.; Kim, J.S. The enhancement of luminescence in Co-doped cubic Eu_2O_3 using Li^+ and Al^{3+} ions. *J. Lumin.* **2011**, *131*, 2597–2605. [CrossRef]
40. Reshak, A.H.; Alahmed, Z.A.; Bila, J.; Atuchin, V.V.; Bazarov, B.G.; Chimitova, O.D.; Molokeev, M.S.; Prosvirin, I.P.; Yelisseyev, A.P. Exploration of the electronic structure of monoclinic α-$Eu_2(MoO_4)_3$: DFT-based study and X-ray photoelectron spectroscopy. *J. Phys. Chem. C* **2016**, *120*, 10559–10568. [CrossRef]
41. Venkatesan, A.; Chandar, N.R.K.; Kandasamy, A.; Chinnu, M.K.; Marimuthu, K.N.; Kumar, R.M.; Jayavel, R. Luminescence and electrochemical properties of rare earth (Gd, Nd) doped V_2O_5 nanostructures synthesized by a non-aqueous sol–gel route. *RSC Adv.* **2015**, *5*, 21778–21785. [CrossRef]
42. Felhi, H.; Smari, M.; Bajorek, A.; Nouri, K.; Dhahri, E.; Bessais, L. Controllable synthesis, XPS investigation and magnetic property of multiferroic $BiMn_2O_5$ system: The role of neodyme doping. *Prog. Nat. Sci. Mater. Int.* **2019**, *29*, 198–209. [CrossRef]
43. Tian, Z.; Zhang, J.; Zhang, T.; Ren, X.; Hu, W.; Zheng, L.; Wang, J. Towards thermal barrier coating application for rare earth silicates RE_2SiO_5 (RE = La, Nd, Sm, Eu, and Gd). *J. Eur. Ceram. Soc.* **2019**, *39*, 1463–1476. [CrossRef]
44. Atuchin, V.; Kesler, V.; Maklakova, N.Y.; Pokrovsky, L.; Sheglov, D. Core level spectroscopy and RHEED analysis of $KGd_{0.95}Nd_{0.05}(WO_4)_2$ surface. *Eur. Phys. J. B-Condens. Matter Complex Syst.* **2006**, *51*, 293–300. [CrossRef]
45. Atuchin, V.; Gavrilova, T.; Grivel, J.C.; Kesler, V. Electronic structure of layered titanate $Nd_2Ti_2O_7$. *Surf. Sci.* **2008**, *602*, 3095–3099. [CrossRef]
46. Atuchin, V.V.; Subanakov, A.; Aleksandrovsky, A.; Bazarov, B.; Bazarova, J.; Dorzhieva, S.; Gavrilova, T.; Krylov, A.; Molokeev, M.; Oreshonkov, A.; et al. Exploration of structural, thermal, vibrational and spectroscopic properties of new noncentrosymmetric double borate $Rb_3NdB_6O_{12}$. *Adv. Powder Technol.* **2017**, *28*, 1309–1315. [CrossRef]
47. Gedekar, K.; Wankhede, S.; Moharil, S.; Belekar, R. d–f luminescence of Ce^{3+} and Eu^{2+} ions in $BaAl_2O_4$, $SrAl_2O_4$ and $CaAl_2O_4$ phosphors. *J. Adv. Ceram.* **2017**, *6*, 341–350. [CrossRef]
48. Atuchin, V.; Isaenko, L.; Kesler, V.; Lin, Z.; Molokeev, M.; Yelisseyev, A.; Zhurkov, S. Exploration on anion ordering, optical properties and electronic structure in $K_3WO_3F_3$ elpasolite. *J. Solid State Chem.* **2012**, *187*, 159–164. [CrossRef]
49. Ji, H.; Huang, Z.; Xia, Z.; Molokeev, M.S.; Jiang, X.; Lin, Z.; Atuchin, V.V. Comparative investigations of the crystal structure and photoluminescence property of eulytite-type $Ba_3Eu(PO_4)_3$ and $Sr_3Eu(PO_4)_3$. *Dalton Trans.* **2015**, *44*, 7679–7686. [CrossRef]
50. Dorenbos, P. Energy of the first $4f^7 \rightarrow 4f^6 5d$ transition of Eu^{2+} in inorganic compounds. *J. Lumin.* **2003**, *104*, 239–260. [CrossRef]
51. Xia, Z.; Zhang, Y.; Molokeev, M.S.; Atuchin, V.V. Structural and luminescence properties of yellow-emitting $NaScSi_2O_6$:Eu^{2+} phosphors:Eu^{2+} site preference analysis and generation of red emission by codoping Mn^{2+} for white-light-emitting diode applications. *J. Phys. Chem. C* **2013**, *117*, 20847–20854. [CrossRef]
52. Ji, H.; Huang, Z.; Xia, Z.; Molokeev, M.S.; Atuchin, V.V.; Fang, M.; Huang, S. New yellow-emitting whitlockite-type structure $Sr_{1.75}Ca_{1.25}(PO_4)_2$:$Eu^{2+}$ phosphor for near-UV pumped white light-emitting devices. *Inorg. Chem.* **2014**, *53*, 5129–5135. [CrossRef]
53. Adachi, S. Review–Photoluminescence Spectroscopy of Eu^{2+}-Activated Phosphors: From Near-UV to Deep Red Luminescence. *ECS J. Solid State Sci. Technol.* **2023**, *12*, 016002. [CrossRef]
54. Ji, H.; Huang, Z.; Xia, Z.; Molokeev, M.S.; Atuchin, V.V.; Huang, S. Cation substitution dependent bimodal photoluminescence in whitlockite structural $Ca_{3-x}Sr_x(PO_4)_2$:Eu^{2+} ($0 \leqslant x \leqslant 2$) solid solution phosphors. *Inorg. Chem.* **2014**, *53*, 11119–11124. [CrossRef] [PubMed]
55. Wang, Z.; Xia, Z.; Molokeev, M.S.; Atuchin, V.V.; Liu, Q. Blue-shift of Eu^{2+} emission in $(Ba,Sr)_3Lu(PO_4)_3$:Eu^{2+} eulytite solid-solution phosphors resulting from release of neighbouring-cation-induced stress. *Dalton Trans.* **2014**, *43*, 16800–16804. [CrossRef] [PubMed]
56. Pei, P.; Liu, K.; Ju, Z.; Wei, R.; Liu, W. Achieving mechano-upconversion-downshifting-afterglow multimodal luminescence in Pr^{3+}/Er^{3+} coactivated $Ba_2Ga_2GeO_7$ for multidimensional anticounterfeiting. *J. Mater. Chem. C* **2022**, *10*, 5240–5248. [CrossRef]
57. Sawada, K.; Nakamura, T.; Adachi, S. Synthesis and properties of $Ca_3Ga_2Ge_3O_{12}$:Tb^{3+} garnet phosphor. *Ceram. Int.* **2017**, *43*, 14225–14232. [CrossRef]
58. Wang, J.; Wang, S.; Su, Q. Synthesis, photoluminescence and thermostimulated-luminescence properties of novel red long-lasting phosphorescent materials β-$Zn_3(PO_4)_2$:Mn^{2+}, M^{3+} (M = Al and Ga). *J. Mater. Chem.* **2004**, *14*, 2569–2574. [CrossRef]
59. Lei, B.; Zhang, H.; Mai, W.; Yue, S.; Liu, Y.; Man, S.Q. Luminescent properties of orange-emitting long-lasting phosphorescence phosphor Ca_2SnO_4:Sm^{3+}. *Solid State Sci.* **2011**, *13*, 525–528. [CrossRef]
60. Urbach, F. Zur lumineszenz der alkalihalogenide. *Sitzungsberichte Akad. Wiss. Wien* **1930**, *139*, 363–372.
61. Chen, D.; Zhou, Y.; Xu, W.; Zhong, J.; Huang, P. Persistent and photo-stimulated luminescence in Ce^{3+}/Cr^{3+} activated $Y_3Al_2Ga_3O_{12}$ phosphors and transparent phosphor-in-glass. *J. Mater. Chem. C* **2016**, *4*, 11457–11464. [CrossRef]
62. Shalgaonkar, C.; Narlikar, A. A review of the recent methods for determining trap depth from glow curves. *J. Mater. Sci.* **1972**, *7*, 1465–1471. [CrossRef]